Int J Ind Chem
DOI 10.1007/s40090-016-0101-0

RESEARCH

Chemical modification at the surface and corrosion inhibition response of two semicarbazones on carbon steel in HCl medium

Vinod Raphael Palayoor[1] · Joby Thomas Kakkassery[2] · Shaju Shanmughan Kanimangalath[1] · Sini Varghese[2]

Received: 24 January 2016 / Accepted: 21 September 2016

Abstract Two similarly structured heterocyclic semicarbazones (E)-4-(5-((2-carbamoylhydrazano)methyl)furan-2-yl)benzoic acid (CPFASC) and (E)-2-((5-(4-nitrophenyl)-furan-2-yl)methylene)hydrazinecarboxamide (NPFASC) were synthesized, characterized and tested for their corrosion protection capacity on carbon steel (CS) in 1 M HCl solution. Contrary to expectation the non-planar molecule NPFASC showed better inhibition efficiency on CS surface than CPFASC. At a concentration of 0.5 mM, NPFASC displayed 93.4 % while CPFASC showed 89.9 % inhibition efficiency according to impedance studies. This unusual behavior can be explained by the conversion of the nitro group present in the NPFASC molecule into amino group on approaching the metal surface in the corrosive medium. This transformation obviously changes the geometry of the molecule which is more conducive for corrosion inhibition. Analysis of the corrosion product deposited on the surface of the metal revealed the mechanism behind the inhibitive power of molecules. Adsorption studies showed that CPFASC and NPFASC follow Freundlich and El-Awady isotherms, respectively, on the carbon steel surface. Adsorption equilibrium constant and free energy of adsorption were also evaluated. The corrosion investigations were done by gravimetric, EIS and polarization studies and the surface analysis of the metal specimens was performed by SEM, AFM and IR spectral spectroscopy.

✉ Joby Thomas Kakkassery
drjobythomask@gmail.com

[1] Department of Chemistry, Government Engineering College, Thrissur 680009, Kerala, India

[2] Research Division, Department of Chemistry, St. Thomas' College (Autonomous), Thrissur 680001, Kerala, India

Keywords Inhibitor · EIS · Polarization · Freundlich · El-Awady

Introduction

The use of corrosion inhibitors is the most practical method to control the metallic dissolution in acidic media and is widely employed in industrial processes like de-scaling, acid pickling, oil well acidizing, etc. Molecules equipped with active corrosion inhibition sites such as hetero atoms like O, S, N, aromatic rings and Schiff bases are found to act as efficient corrosion inhibitors in aggressive media [1–7]. A few semicarbazones and hydrazones exhibited good corrosion protection ability due to the presence of C=N group [11, 16]. Electronic effects such as inductive, mesomeric, etc., affect the corrosion inhibition power of molecules. Scientists and industrialists are ever in search of soluble, durable and economic corrosion inhibitors. Many researchers are trying to substantiate the mechanism behind corrosion inhibition of organic molecules on various metals using experimental as well as quantum chemical methods. The corrosion inhibition response of a molecule is closely related to its structure and geometry [8, 9]. The reactions of the inhibitor molecules with aggressive medium may also influence the behavior of the molecules. This type of response of the molecules has to be taken into account when one explains the mechanism of corrosion inhibition. For instance, the behavior of the Schiff base *N*,*N*′-bis(salicylidene)-1,2-ethylenediamine (Salen) and a mixture of its parent molecules, ethylenediamine and salicylaldehyde, as carbon steel corrosion inhibitors in 1 M HCl solution was studied by da Silva et al. [10] using corrosion potential measurements, potentiodynamic polarization curves, electrochemical impedance spectroscopy and spectrophotometric measurements. They reported that results

Published online: 15 October 2016

obtained in the presence of Salen were similar to those obtained in the presence of the salicylaldehyde and ethylenediamine mixture, showing that in acid medium the Salen molecule undergoes hydrolysis, regenerating its precursor molecules. In one of previous studies, we could establish the corrosion antagonistic behavior of 3-acetylphenylhyrazone (3APPH) on carbon steel in 0.5 M H_2SO_4. The corrosion rate of CS increased with the concentration of 3APPH. Intense hydrolysis to this molecule occurred in sulphuric acid, which was confirmed by UV–visible spectroscopy. The same compound showed very high inhibition efficiency (>99 % at 1.0 mM as per electrochemical studies) on CS surface in 0.5 M H_2SO_4 in the presence of trace amount of KI [11]. It is quite sure that the corrosion inhibiting capacity of a molecule is a combined effect of its molecular structure, geometry and the way in which it behaves in the aggressive medium in the presence of a metal.

In the present course of study, we synthesized two furan-2-aldehyde derived semicarbazones and investigated their corrosion inhibition response on carbon steel in 1 M HCl using gravimetric, surface and electrochemical analytical techniques. The major aim was to relate the structural behavior of the molecules with its corrosion inhibition capacity and to explore the combined influence of the aggressive medium and metal in modifying the performance of the molecules.

Experimental

Synthesis and characterization of semicarbazones

All chemicals for synthesis were purchased from Merck Millipore. Furan-2-aldehyde (98 %), p-aminobenzoic acid (>99 %), $NaNO_2$ (EMSURE®), p-nitroaniline (>99 %), $CuCl_2{\cdot}2H_2O$ (EMSURE®) and semicarbazide hydrochloride (>99 %) were used for synthesis.

Semicarbazones were synthesized in two steps, i.e., arylation of furan-2-aldehyde (Meerwein arylation) followed by the condensation reaction with semicarbazide. Meerwein arylation was conducted by standard method, reported elsewhere [12]. For this, 10 mmol of p-aminobenzoic acid/p-nitroaniline was diazotized at 0–5 °C using $NaNO_2$ and HCl. The reaction mixture was kept for 20 min and equimolar amount of furan-2-aldehyde in acetone followed by 3 mmol of $CuCl_2{\cdot}2H_2O$ in water were added. The entire reaction mixture was kept for 2 days with occasional shaking. The precipitated yellow colored solid was filtered, washed with warm water and dried.

The arylated furfural derivative was dissolved in ethanol and heated to reflux in a water bath. Equimolar amount of semicarbazide hydrochloride was dissolved in ethanol water mixture (9:1) and added drop-wise into the boiling solution. The mixture was kept for 12 h and the precipitated compound was filtered, washed with ethanol–water mixture (1:1) and dried. Figure 1 shows the reaction pathway for the synthesis of semicarbazones. The products were characterized by elemental (Elementar make Vario EL III-CHN analyzer) analysis and mass (Shimadzu, QP 2010 GCMS), nmr (Bruker Avance III HD—dmso-d_6 solvent), UV–visible (Shimadzu UV–visible-1800 Spectrophotometer—DMSO solvent) and IR (Shimadzu Affinity-1-KBr pellet method) spectroscopic analyses.

Metal specimen and aggressive medium

Carbon steel coupons having 0.58 % Mn, 0.07 % P, 0.02 % S, 0.015 % Si, 0.02 % and the rest Fe (estimated by EDAX technique-SEM, Hitachi SU6600 model) were cut (1.5 × 1.5 × 0.15 cm) and polished with various grades of emery papers (120, 400, 600, 800, 1000 and 1200). The specimens were washed with soap solution, degreased with acetone, dried in air oven and weighed [13]. A stock solution of CPFASC and NPFASC (0.5 mM) was prepared in 1 M HCl. This solution was diluted with 1 M HCl to get the inhibitor solutions in the range 0.1–0.5 mM.

Gravimetric corrosion studies

CS specimens were carefully hanged using polyethylene fishing lines in 1 M HCl in the presence of various concentrations of semicarbazones for 24 h at RT (29 ± 0.1 °C). Blank experiment was also conducted in the

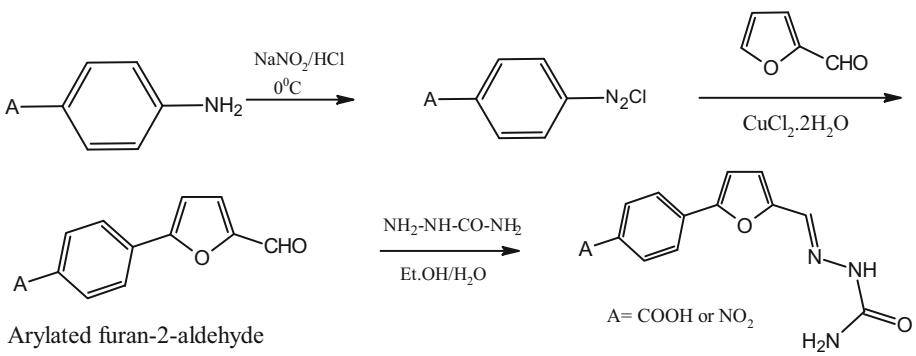

Arylated furan-2-aldehyde

Fig. 1 Reaction pathway for the synthesis of semicarbazones

absence of semicarbazones. Total volume of the aggressive medium was 50 ml in each experiment. From the initial and final weight of the metal specimen, the rate of corrosion was determined using the following equation

$$\upsilon = \frac{KW}{DSt}, \quad (1)$$

where υ corrosion rate (mm year^{-1}), W weight loss (g), S surface area of metal specimen (cm^2), t time of treatment (h), D density of specimen (g cm^{-3}) and K a constant (8.76×10^4). The inhibition efficiency (η_w %) was obtained by the following equation [14–16].

$$\eta_w\,\% = \frac{\upsilon - \upsilon'}{\upsilon} \times 100, \quad (2)$$

where υ and υ' are the corrosion rate of the CS specimen in the absence and presence of the inhibitor, respectively. For good reproducibility, all the experiments were conducted in duplicate and the average values were taken.

Electrochemical corrosion investigations

Three-electrode circuitry was used for electrochemical investigations. Saturated calomel electrode (SCE) and platinum electrode with 1 cm^2 surface area acted as reference and counter electrodes, respectively. Polished metal specimen exposed to the aggressive solution with an area of 1 cm^2 acted as working electrode. The working electrode was kept in contact with the aggressive solution to attain steady-state open-circuit potential (OCP). Each metal specimen was immersed in the aggressive medium for a period of 30 min prior to the experiment at 29 °C. The electrochemical studies were carried out by Ivium compactsat-e electrochemical system (Netherlands) controlled by Ivimsoft software. Impedance spectroscopic studies were conducted to evaluate the corrosion inhibition efficiency of the heterocyclic molecules. A frequency range of 1 kHz–100 mHz with an amplitude of 10 mV as excitation signal was used for every experiment [17]. Analysis of impedance plots provided the charge transfer resistance by which one can measure the corrosion inhibition efficiency using following equation [18].

$$\eta_{EIS}\,\% = \frac{R_{ct} - R'_{ct}}{R_{ct}} \times 100, \quad (3)$$

where R_{ct} and R'_{ct} are the charge transfer resistances of working electrode with and without inhibitor, respectively.

Tafel polarization studies were executed between +100 and −100 mV with a sweep rate of 1 mV/s at RT (29 ± 0.1 °C). Analysis of Tafel lines gave corrosion current densities by which inhibition efficiency was calculated using the following equation [19, 20]:

$$\eta_{pol}\,\% = \frac{I_{corr} - I'_{corr}}{I_{corr}} \times 100, \quad (4)$$

where I_{corr} and I'_{corr} are the uninhibited and inhibited corrosion current densities, respectively.

Surface analysis

The deposited film of semicarbazone on CS surface was scrapped and analyzed with IR spectroscopy (Shimadzu Affinity-1-KBr pellet method). Morphology of metal surface was studied by SEM (Hitachi SU6600 model). Topography of the CS specimens was monitored by AFM (Park Systems XE-100 model) in the contact mode. Scanning of specimens in the area 5 × 5 μm at a rate of 0.8 Hz provided the topographic images.

Results and discussion

Structure of semicarbazones

Melting point, elemental data and spectral analytical data of CPFASC and NPFASC are shown in the subsequent paragraphs.

CPFASC: M. P. 290 °C, CHN found (calc.): C %; 55.85 (57.14 %), H %; 4.14 (4.03), N %; 14.44 (15.38), Mass spectrum; M + peak m/z = 273, base peak m/z = 230 ($[C_{12}H_{10}N_2O_3]^+$), ^{1}Hnmr spectrum; 10.3 δ (COOH), 7.73 δ(s), (CH=N) 6.38δ (s,br) (NH). ^{13}Cnmr spectrum; 166.87 ppm (COOH), 152.55 ppm (CH=N), IR spectrum; 1666 cm^{-1} (C=N), 3477 cm^{-1} (OH), 3363 cm^{-1} (NH), UV–vis spectrum; 27,777 cm^{-1} (n → π*), 28,490 cm^{-1} (π → π*).

NPFASC: M. P. 221 °C, CHN found (calc.): C %; 52.78 (52.55), H %; 3.99 (3.65), N %; 21.01 (20.43). Mass spectrum; M + peak *m/z* = 274, base peak *m/z* = 231 ($[C_{11}H_9O_3N_3]^+$), ^{1}Hnmr spectrum; 8.36 δ(s) (CH=N), 6.41 δ(s,br) (NH), ^{13}Cnmr spectrum; 154.21 ppm (CH=N), IR spectrum; 1693 cm^{-1} (C=O), 1597 cm^{-1} (C=N), UV–vis spectrum; 29,615 cm^{-1} (n → π*), 32,011 cm^{-1} (π → π*).

The structures and optimized geometries of the molecules CPFASC, NPFASC and the reduced form of NPFASC (APFASC—will be discussed later) are given in Fig. 2.

Gravimetric corrosion studies

The corrosion inhibition efficiencies of heterocyclic semicarbazones on CS for a period of 24 h are listed in Table 1. According to gravimetric studies, both molecules appreciably prevented the metallic dissolution in the aggressive medium and the inhibition efficiency increased with the

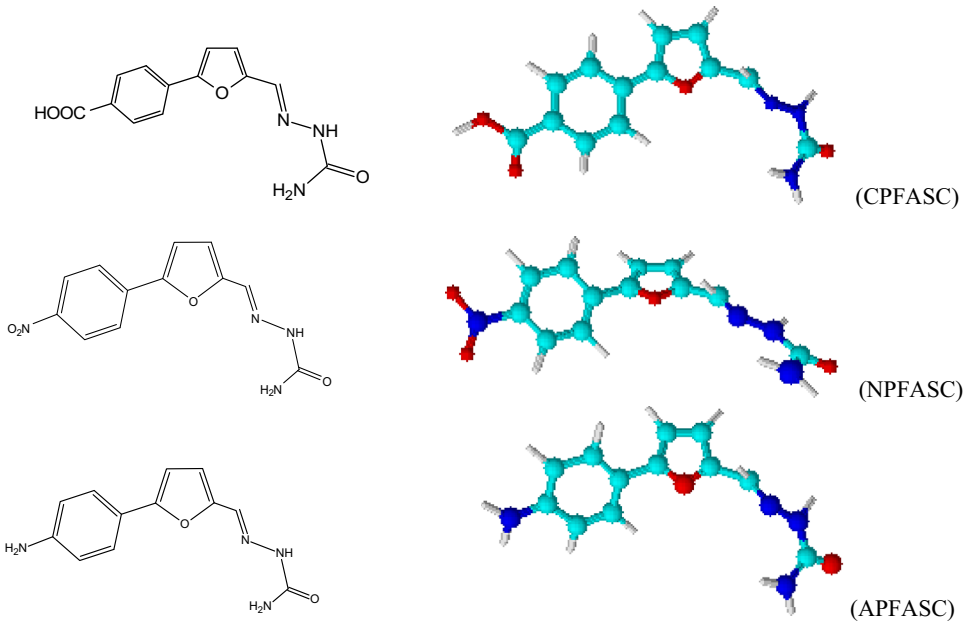

Fig. 2 Structures and optimized geometries of semicarbazones

Table 1 Corrosion inhibition efficiencies (η_w %) of CPFASC and NPFASC on CS in 1 M HCl for 24 h at 29 °C

C (mM)	CPFASC	NPFASC
0.1	25.88	36.54
0.2	43.24	44.68
0.3	58.72	77.83
0.4	74.54	78.75
0.5	84.37	85.44

concentration. At 0.5 mM, both molecules displayed >80 % inhibition efficiency. Among the semicarbazones CPFASC and NPFASC, former one displayed lesser efficiency than latter on CS surface in acidic medium at all concentrations.

The only difference between the structures of CPFASC and NPFASC is that CPFASC contains a –COOH group attached to the phenyl ring instead, $–NO_2$ group is attached to the phenyl ring in NPFASC. While explaining the corrosion inhibition efficiency of molecules in terms of their structures, it is important to point out two factors: (1) the electron denser sites on the molecule and (2) geometry of the molecule. On comparing the structures of CPFASC and NPFASC, evidently, the electron density of the aromatic rings and azomethine linkage will be poorer in NPFASC than in CPFASC due to the presence of highly electron withdrawing $–NO_2$ group and the NPFASC molecule is expected to display inferior corrosion inhibition efficiency than CPFASC. Moreover, considerable deviation can be observed from co-planarity in optimized geometry of NPFASC (Fig. 2), which is an unfavorable scenario for the firm interaction of molecules on the metal surface. Contrary to expectation, NPFASC molecule showed better corrosion inhibition efficacy than CPFASC at all concentrations. This unusual behavior can be accounted by Bechamp's reduction, i.e., reduction of nitro group of the molecule into amino group in the presence of Fe and HCl [21], which can be seen from Fig. 3.

The possibility for the reduction of large number of NPFASC into APFASC in HCl medium is high when the molecules approach the metal surface, which helps to improve the corrosion inhibition efficacy of the NPFASC molecule appreciably than CPFASC molecule. Upon reduction, the electron density of the phenyl ring, furan ring and the azomethine linkage increases significantly. This is because, the electron deactivating nitro group is replaced by electron-rich amino group. The amino group of APFASC can donate the lone pair of electron to the vacant molecular orbitals of Fe. The free electron pair can also participate in resonance which will definitely improve the electron richness of the aromatic ring. Furthermore, the reduced molecule gets a complete planar structure (Fig. 2) according to the optimized geometry. Now, these reduced molecules can interact with the metal surface more effectively than before and thus prevent the metal dissolution more efficiently. Very strong evidence regarding the reduction of NPFASC is obtained from the mass spectral analysis of the film formed on CS surface and the spectrum exhibited a clear signal at *m/z* 244, which is the exact molecular mass of the reduced NPFASC, i.e., APFASC. This peak was not seen in the mass spectrum of NPFASC. The signal due to the molecular ion peak of NPFASC (m/z = 274), which was totally absent in the mass spectrum of the corrosion product, indicates the absence of free NPFASC molecules in the corrosion product. Figure 4 shows the mass spectrum of NPFASC and the surface film

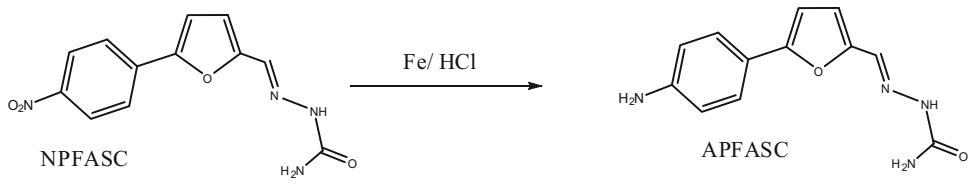

Fig. 3 Conversion of NPFASC into APFASC in the presence of Fe and HCl

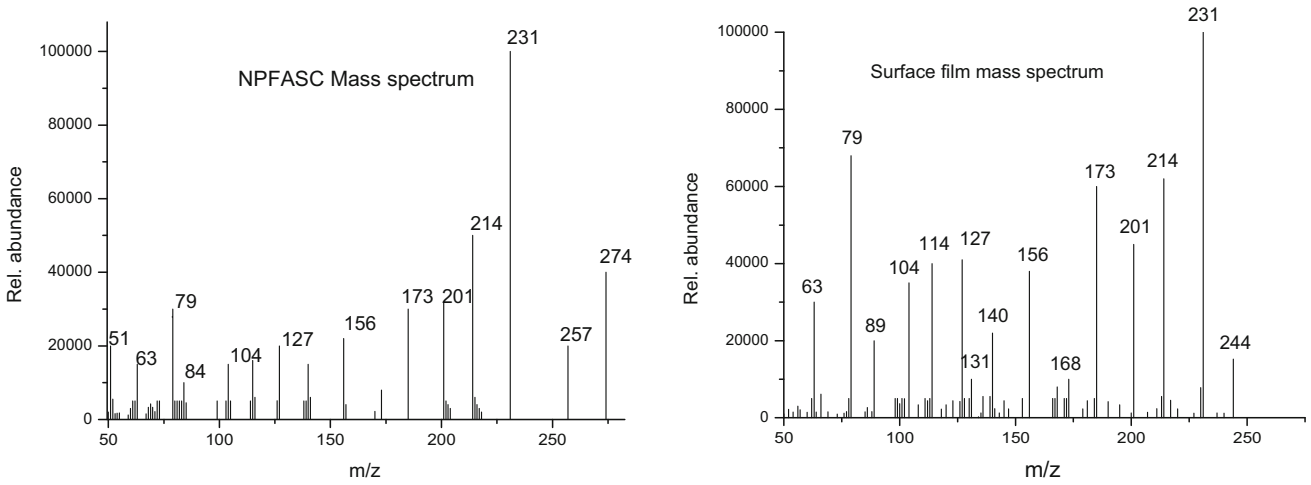

Fig. 4 Mass spectrum of NPFASC and surface film on CS treated with NPFASC (0.5 mM) in 1 M HCl for 24 h

formed on CS after the treatment with NPFASC (0.5 mM) in 1 M HCl for 24 h at 29 °C. The overall mechanism of interaction of NPFASC on CS in 1 M HCl can be visualized from Fig. 5.

Adsorption isotherms

To get more insight into the mechanism of corrosion, adsorption isotherms were plotted. Among the various isotherm models tried, the most suitable one was selected with the help of regression coefficient (Table 2). The most fit isotherm model for CPFASC and NPFASC on CS in 1 M HCl was Freundlich and El-Awady isotherm (Eqs. 5, 6) [22–24], where θ is fractional surface coverage, K_{ads} is the adsorption equilibrium constant and C is the concentration of the inhibitor. In El-Awady isotherm, $K_{ads} = K^{1/y}$. The regression coefficient of El-Awady isotherm for NPFASC/APFASC system on CS surface was 0.899. Considerable deviation from unity of this isotherm may be due to the adsorption of two different molecules (NPFASC and APFASC) at the same time on CS surface. The adsorption equilibrium constant for CPFASC was 1515 while that of NPFASC/APFASC was 6130, indicating the elevated interaction of latter molecules on CS surface. The free energies of adsorption (ΔG_{ads}) calculated by Eq. 7 were −28.6 and −31.9 kJ mol^{-1}, respectively, for CPFASC and NPFASC/APFASC on CS surface. Generally, the values of ΔG_{ads} up to −20 kJ/mol is an indication of electrostatic interaction (physisorption) of charged molecules and the metal, while those around −40 kJ mol^{-1} stands for chemisorption. Since the ΔG_{ads} values lie between −20 and −40 kJ mol^{-1}, for CPFASC and NPFASC, both physisorption and chemisorption were involved during the interaction of molecules on CS surface [25]. The involvement of chemical force was much higher in the case of NPFASC/APFASC than CPFASC on CS surface as evident from the free energy values. On analyzing the structures of the CPFASC and NPFASC, it may be assumed that the aromatic ring systems, azomethine linkage and the nitrogen atoms of semicarbazide part are the active sites of adsorption. But the transformation of NPFASC into APFASC led to the generation of an additional electron-rich site (amino group) in APFASC. Moreover, the electron density of the aromatic rings and azomethine linkage escalated due to the transformation of NPFASC into APFASC in the presence of Fe and HCl.

Figure 6a, b shows adsorption isotherms for CPFASC and NPFASC on CS surface in 1 M HCl, respectively.

$$\text{Freundlich adsorption isotherm } \theta = K_{ads}C \tag{5}$$

$$\text{El} - \text{Awady adsorption isotherm } \log\left(\frac{\theta}{1-\theta}\right) = \log K + y\log C \tag{6}$$

$$\Delta G_{ads} = -2.303RT\log(55.85K_{ads}) \tag{7}$$

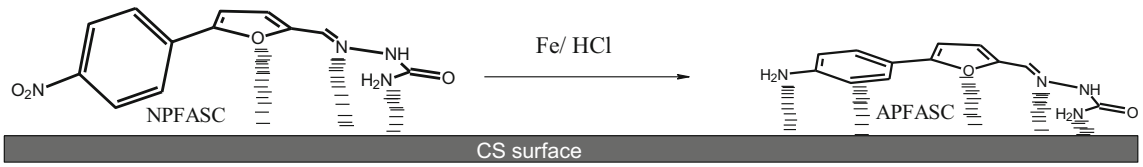

Fig. 5 Illustration of the interaction of NPFASC on CS surface in 1 M HCl

Table 2 Adsorption isotherm models and their regression coefficients for CPFASC and NPFASC on CS in 1 M HCl

Adsorption isotherm	CPFASC	NPFASC
Langmuir	0.973	0.828
Freundlich	0.991	0.872
Temkin	0.973	0.893
Flory–Huggin	0.888	0.555
El-Awady	0.960	0.899

Electrochemical studies

Figure 7a, b represents the Nyquist plots of metal specimens treated with CPFASC and NPFASC, respectively, in acidic medium. The impedance parameters are listed in Table 3. From the figures and table it is evident that the R_{ct} values increased with the concentration of the semicarbazones, which shows the reluctance of metal dissolution with the inhibitor concentration. The solution resistance values did not show appreciable change with the concentration. The simple equivalent circuit (Randle's equivalent circuit) that fits these electrochemical systems is a parallel combination of double-layer capacitance C_{dl} and charge transfer resistance R_{ct}, both in series with the solution resistance R_s [26, 27]. For instance, Fig. 8a, b shows two simulated EIS spectrum for CS in the presence of CPFASC and NPFASC (0.3 mM) using Iviumsoft program. The red square symbols denote the impedance values and the black line represents the fitting curve. The equivalent circuit is also provided in the figures. From the figures it is evident that the Randle's equivalent circuit is the best circuit that would fit for the measured impedance. Bode plots for various concentrations of CPFASC and NPFASC are given in Fig. 9a, b.

Nyquist plots were not perfect semicircles, which may be attributed to the nonhomogeneity of the CS surface, grain boundaries and impurities [28]. To get an accurate fit, constant phase element (CPE) was introduced in the circuit than pure double-layer capacitor. The impedance of CPE can be represented as [29]

$$Z_{CPE} = \frac{1}{Y_0(j\omega)^n}, \tag{8}$$

where Y_0 is the magnitude of CPE, n is the exponent (phase shift), ω is the angular frequency and j is the imaginary unit. Depending upon the values of n, CPE may be resistive, capacitive and inductive. The capacitive behavior of CPE was established in all analyses since the calculated value of n varied between 0.8 and 0.86 [28]. Since the shapes of Nyquist plots do not change with the concentration of the inhibitor, it can be assumed that the mechanism of corrosion inhibition by the molecules does not alter with the concentration. The charge transfer resistance significantly increased with the concentration of semicarbazones. Even at low concentrations NPFASC exhibited very high corrosion inhibition efficiency and it was greater than that of CPFASC. The double-layer capacitance decreased with the concentration of inhibiting molecules. This is either due to the decrease of local dielectric constant or the increase of thickness of electric double layer (or both) with the adsorption of semicarbazones. It is also

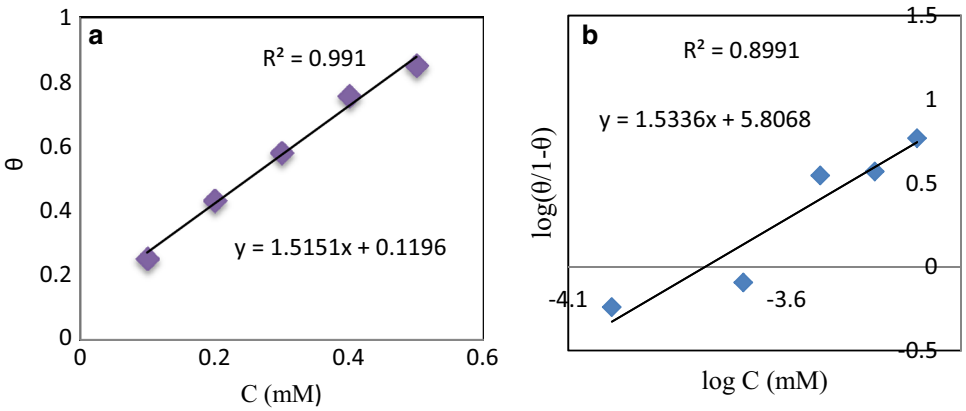

Fig. 6 **a** Freundlich adsorption isotherm for CPFASC and **b** El-Awady adsorption isotherm for NPFASC on CS in 1 M HCl on CS in 1 M HCl

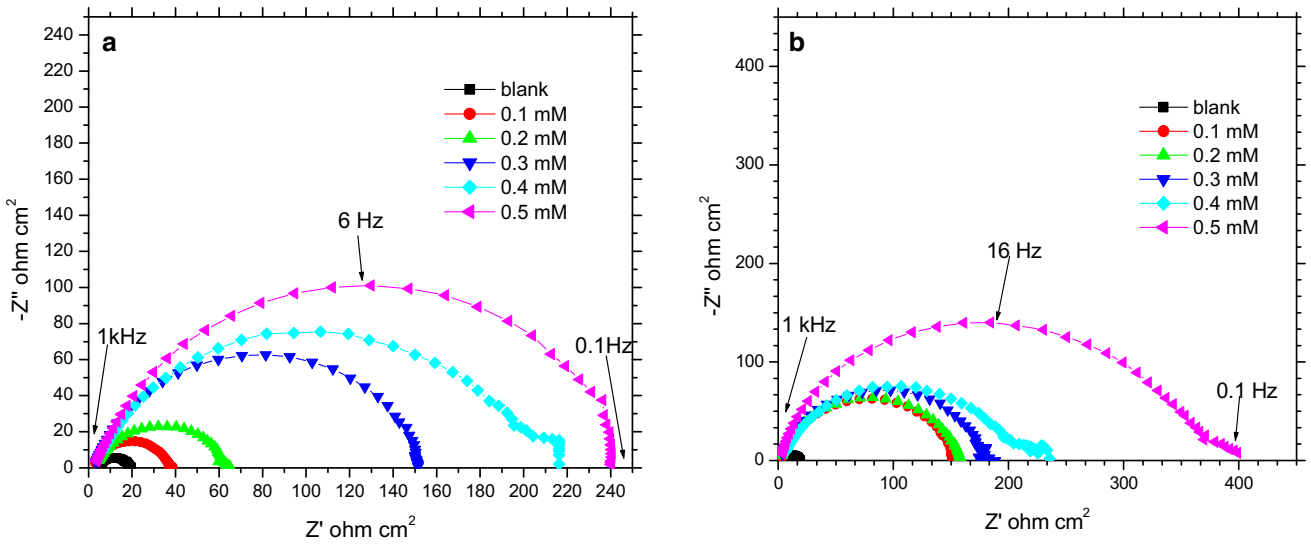

Fig. 7 Nyquist plots of CS in the presence and absence of **a** CPFASC and **b** NPFASC in 1 M HCl at 29 °C

Table 3 Electrochemical impedance and polarization parameters of CS in the presence and absence of semicarbazones CPFASC and NPFASC in 1 M HCl

Semicarbazone	Impedance data					Polarization data				
	C (mM)	C_{dl} (μF cm^{-2})	N	R_{ct} (Ω cm^2)	η_{EIS} %	$-E_{corr}$ (mV)	I_{corr} (μA cm^{-2})	$-b_c$ (mV dec^{-1})	B_a (mV dec^{-1})	η_{pol} %
Blank	0	76.36	0.80	23.08	–	474	499.6	102	77	–
CPFASC	0.1	72.00	0.81	38.96	40.76	474	215.6	54	87	56.85
	0.2	60.69	0.82	55.88	58.70	498	146.0	64	94	70.78
	0.3	58.80	0.82	136.50	83.09	507	102.0	79	93	79.58
	0.4	56.00	0.84	187.80	87.71	493	76.84	77	94	84.62
	0.5	56.10	0.85	227.40	89.85	492	61.9	75	93	87.61
NPFASC	0.1	71.89	0.83	132.80	82.68	489	95.29	82	94	80.93
	0.2	59.37	0.85	134.10	82.85	498	73.12	85	92	85.36
	0.3	54.88	0.83	171.40	86.58	480	66.44	82	86	86.70
	0.4	43.75	0.84	192.40	88.05	487	65.55	78	62	86.88
	0.5	43.67	0.86	350.00	93.40	475	37.36	84	79	92.52

visible from the data that C_{dl} (NPFASC) $<C_{dl}$ (CPFASC) at all concentrations, which implies a better interaction of NPFASC on Fe surface than CPFASC.

Tafel lines of the metal specimens in the presence and absence of the semicarbazones are given in Fig. 10. Polarization parameters like corrosion potential (E_{corr}), corrosion current density (I_{corr}), cathodic slope (b_c), anodic slope (b_a), etc., and inhibition efficiency (η_{pol} %) are represented in the Table 3. From the Tafel data it is evident that NPFASC molecule demonstrated elevated inhibition efficiencies than CPFASC at all concentrations. At a concentration of 0.5 mM, NPFASC displayed 92.5 % inhibition efficiency on CS. Corrosion current densities decreased appreciably with concentration of semicarbazones suggesting that reluctance of the metal dissolution increased with the concentration. On close examination of polarization data one can assure that CPFASC molecule worked more at cathodic regions of corrosion. This was because cathodic slopes were altered considerably when compared to that of blank. Thus the rate of H_2 formation was lowered by CPFASC than the rate of metal dissolution process. The cathodic slopes of Tafel lines in the presence of NPFASC did not change considerably while anodic slopes showed more shifts. This suggests that NPFASC/APFASC molecules were more active at anodic sites of corrosion or metal dissolution process [30, 31]. There was high compatibility between the η_{pol} and η_{EIS} % for the semicarbazones.

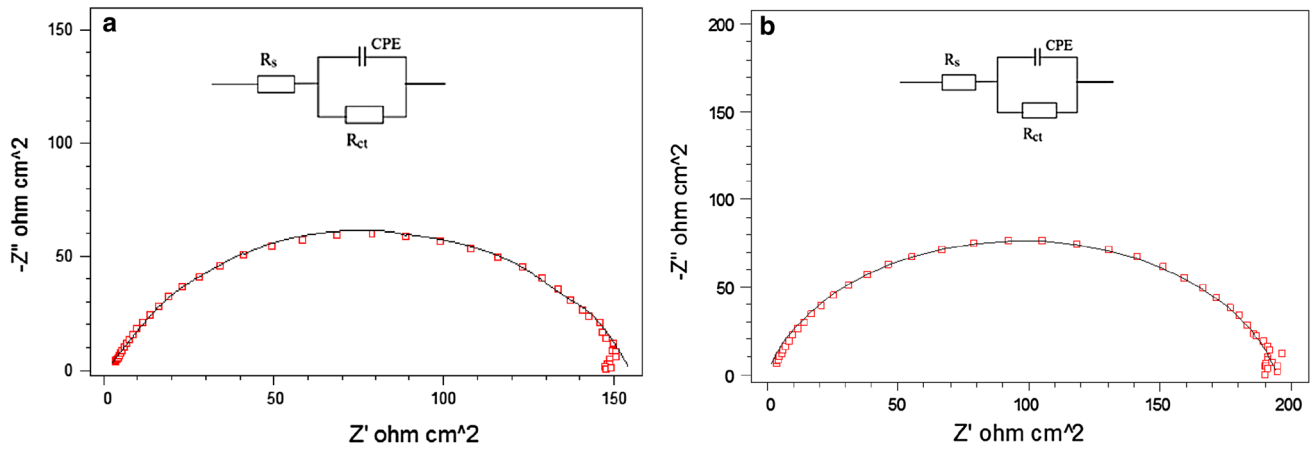

Fig. 8 EIS fitting curves and their corresponding equivalent circuit for CS in the presence of 0.3 mM **a** CPFASC and **b** NPFASC in 1 M HCl at 29 °C

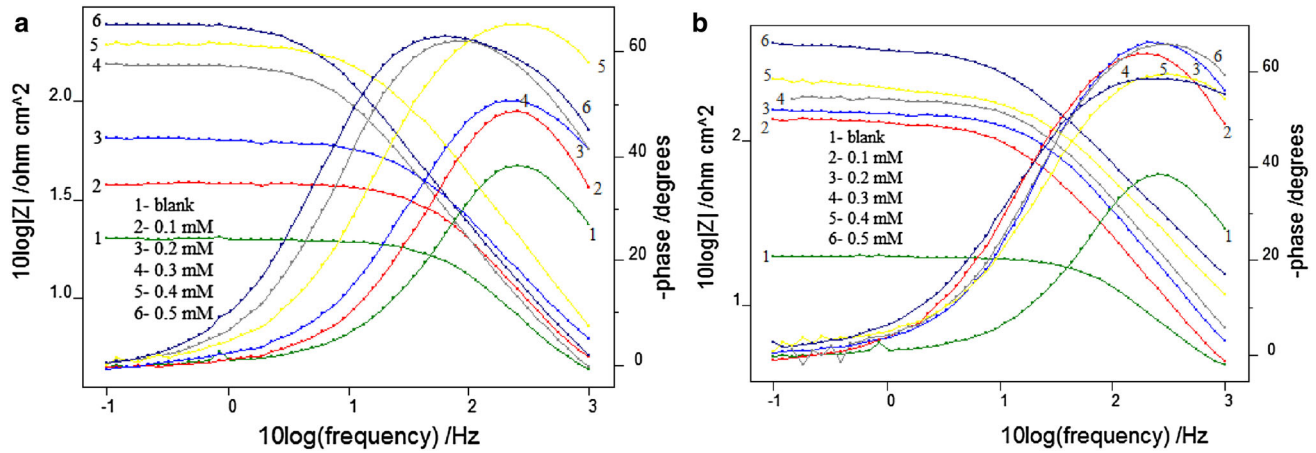

Fig. 9 Impedance and Bode plots of CS in the presence and absence of **a** CPFASC and **b** NPFASC in 1 M HCl at 29 °C

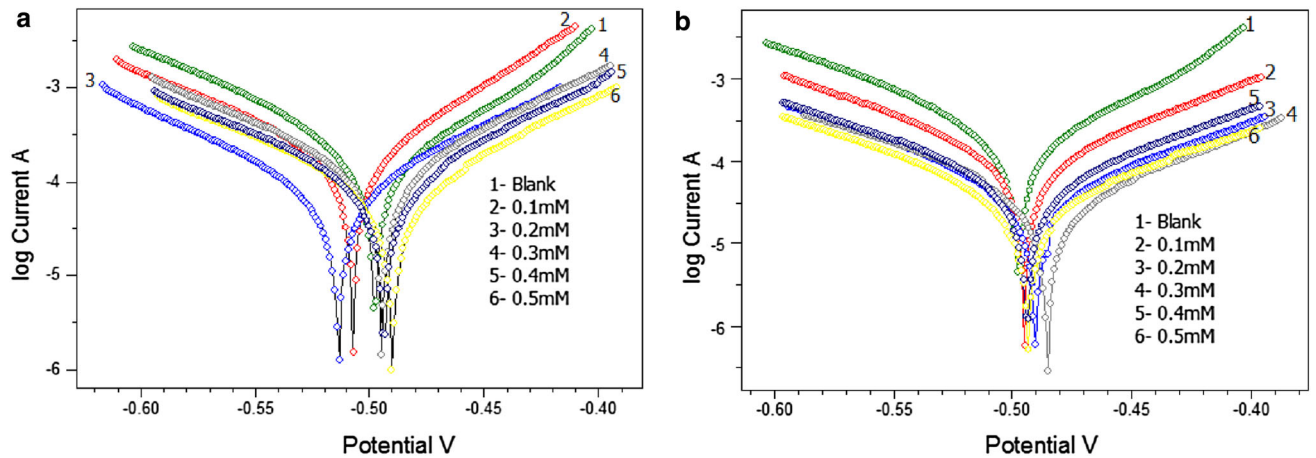

Fig. 10 Tafel plots of CS in the presence and absence of **a** CPFASC and **b** NPFASC in 1 M HCl at 29 °C

Surface analysis

IR spectral studies

The film deposited on the CS surface (treated for 24 h in 1 M HCl in the presence of 0.5 mM semicarbazone) was mechanically removed and subjected to IR spectral analysis. The spectrum was compared with the IR spectrum of the semicarbazone (Fig. 11). The IR spectrum of the surface film was very similar to that of spectrum of CPAFSC. But lowering of frequencies in some regions indicated that the molecules made coordinate type bond with the surface metal atoms. When comparing the spectrum of NPFASC and its surface film, appreciable dissimilarities could be observed. This is an indication of alteration of the basic structure of the adsorbed molecule on the metal surface, i.e., the conversion of NPFASC to APFASC in the presence of Fe and HCl. A sharp peak that appeared at $\sim$3500 cm^{-1} in the spectrum of surface film is assignable to the stretching frequency of newly formed amino group in APFASC. It may be concluded that the surface film IR spectrum of NPFASC is the combined spectrum of adsorbed NPFASC and APFASC on Fe surface. Some of the fundamental frequencies of NPFASC were observed in the spectrum of the surface film. A very strong absorption in the lower region of the IR spectrum ($\sim$800–500 cm^{-1}) of NPFASC film may be attributed to the strong interaction of the molecules with the metal atoms by making coordinate bonds such as Fe–O and Fe–N, etc.

SEM studies

Surface morphological studies of CS specimens were performed using SEM. Figure 12a–d represents the SEM images of metal specimens, i.e., bare, treated with 1 M HCl for 24 h (blank), treated with 0.5 mM CPFASC and 0.5 mM NPFASC in 1 M HCl solution. It was clear that the four surface morphologies were entirely different. The surface of bare specimen was smoother than other specimens. Mild pits and cracks that appeared in the image of bare specimen were due to the effect of polishing. Attack of the aggressive solution on the metal surface made it rough is evident from Fig. 12b. From the surface images, Fig. 12c, d, it can be concluded that heterocyclic hydrazones shield the CS corrosion markedly in acidic medium by forming a protective layer.

AFM studies

Surface interaction of the heterocyclic semicarbazones on CS was further confirmed by AFM studies. Topography of bare specimen, blank, specimens treated with 0.5 mM CPFASC and NPFASC in 1 M HCl for 24 h are given in Fig. 13a–d, respectively. The roughness parameters which characterize the topography of surfaces like average roughness (arithmetic mean of the absolute values of the height of the surface profile, R_a), root mean square roughness (mean squared absolute values of surface roughness profile R_q), ten-point roughness (arithmetic mean of the five highest peaks added to the five deepest valleys over the evaluation length measured R_z) and maximum peak-to-valley height (R_{px}) [32, 33] are provided in Table 4. The roughness parameters for the bare metal specimen were very low due to the smoothness of the surface when compared to the blank specimen, which was in continuous reaction with the aggressive medium. When analyzing the topography of the metal specimens which were in contact with the organic molecules, it is understandable that the roughness parameters lie between the parameters of bare and blank specimens. This is an indication of the adsorption of the molecules on the

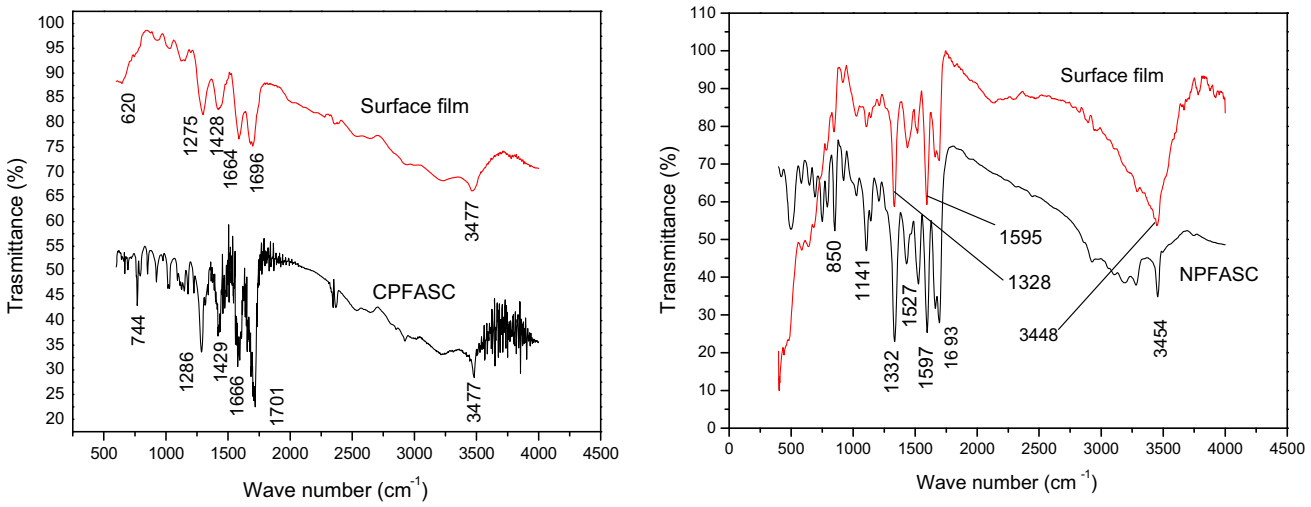

Fig. 11 IR spectra of semicarbazone and the surface film formed on CS in 1.0 M HCl in the presence of 0.5 mM semicarbazone for 24 h

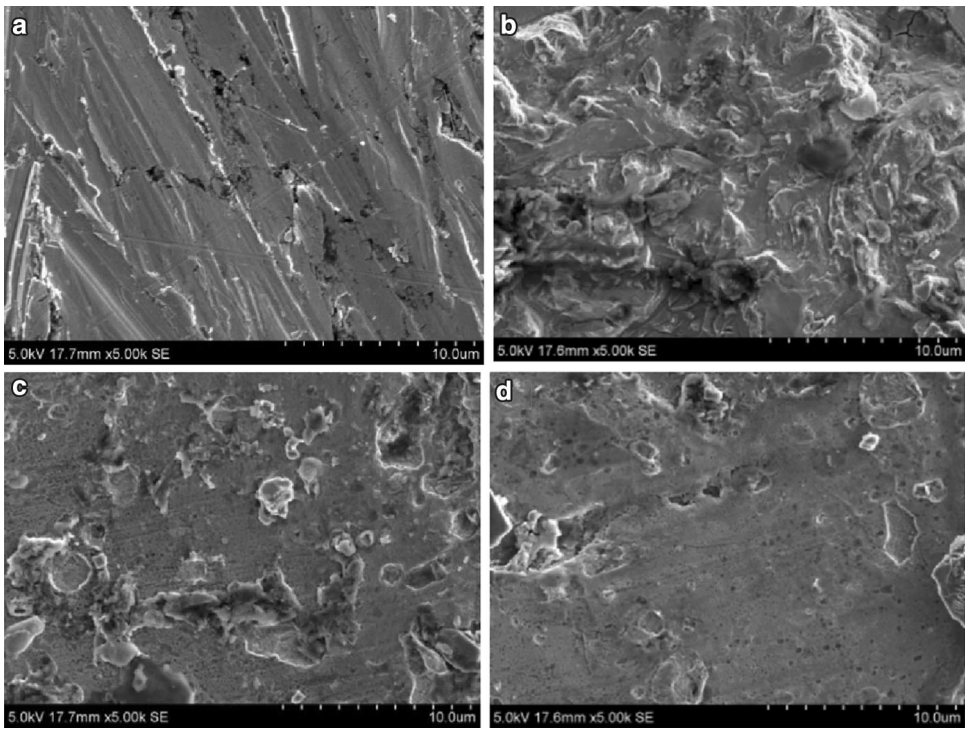

Fig. 12 SEM images of **a** bare CS surface **b** CS treated with 1 M HCl for 24 h **c** CS treated with 1 M HCl in the presence of 0.5 mM CPFASC for 24 h **d** CS treated with 1 M HCl in the presence of 0.5 mM NPFASC for 24 h

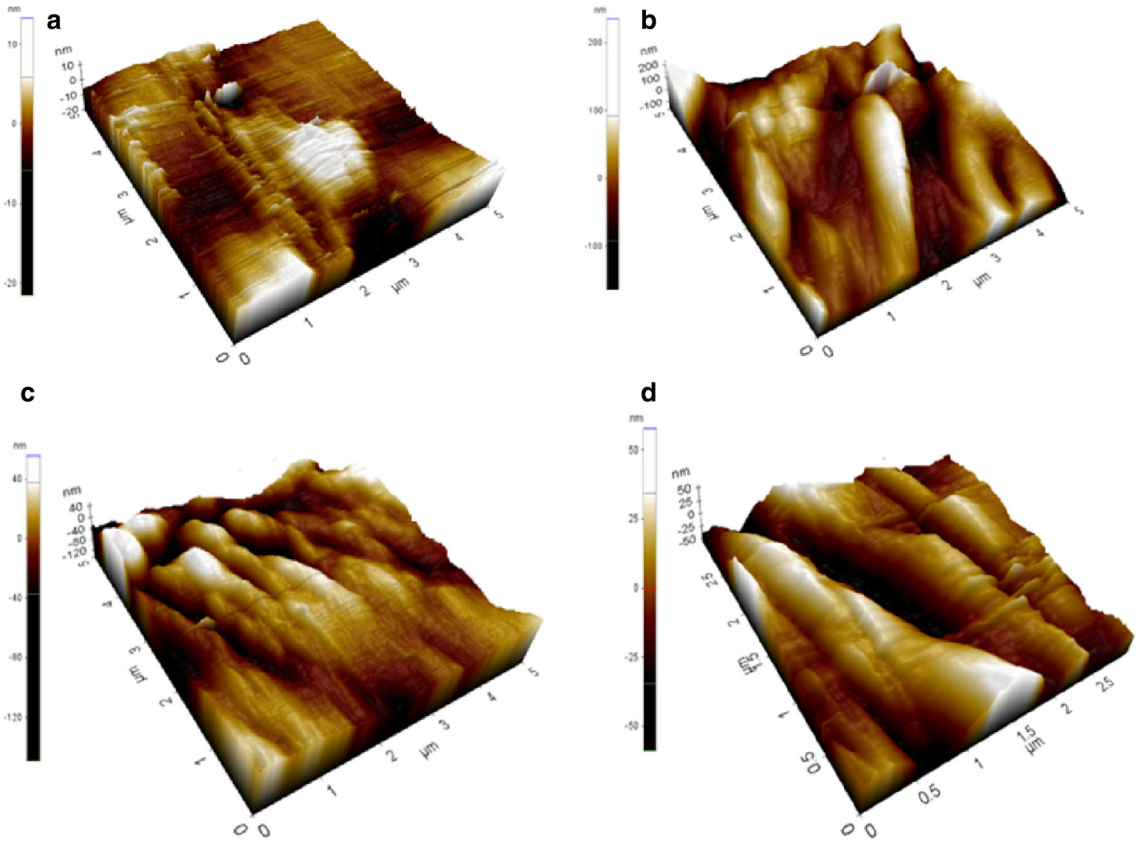

Fig. 13 Topography of **a** bare CS **b** CS treated with 1 M HCl for 24 h **c** CS treated with 1 M HCl in the presence of 0.5 mM CPFASC for 24 h **d** CS treated with 1 M HCl in the presence of 0.5 mM NPFASC for 24 h

Table 4 Roughness parameters of metal specimens by AFM studies

Metal surface	Peak-to-valley height R_{px} (nm)	RMS roughness R_q (nm)	Average roughness R_a (nm)	Ten-point roughness R_z (nm)
Bare metal	34.79	3.02	2.16	30.66
Metal in 1 M HCl (24 h)	399.42	47.11	36.90	380.71
Metal in 1 M HCl with 0.5 mM CPFASC (24 h)	121.77	24.62	16.35	110.24
Metal in 1 M HCl with 0.5 mM NPFASC (24 h)	116.49	17.57	13.80	109.7

metal surface during the dissolution process. It is worthwhile to mention that the AFM parameters of the metal specimen treated with NPFASC are to some extent lower than that of the specimen treated with CPFASC indicating that the former molecule fights well against corrosion than the latter.

Conclusions

The corrosion monitoring studies established that inhibition efficiency of NPFASC is higher than that of CPFASC in 1 M HCl medium, even though the molecule possesses a non-planar geometry and electron withdrawing group. The explanation for the unexpected outcome was the transformation of NPFASC molecule into APFASC in the presence of iron and acid. Mass spectral studies of the surface film confirmed the transformation of NPFASC molecules into APFASC. CPFASC and NPFASC followed Freundlich and El-Awady adsorption isotherms, respectively, on CS surface in HCl medium. Comparatively weak interaction existed between CPFASC and metal surface. Potentiodynamic polarization studies revealed that CPFASC was more active at cathodic sites of corrosion while NPFASC prevented the anodic process of corrosion appreciably. Surface analysis using IR spectroscopy was also performed. The protective layer of inhibiting compounds on CS was visible from the scanning electron micrographs. AFM analysis explored the topography of CS specimens.

References

1. Hosseini M, Mertens SFL, Ghorbani M, Arshadi MR (2003) Asymmetrical Schiff bases as inhibitors of mild steel corrosion in sulphuric acid media. Mater Chem Phy 78(3):800–808
2. Saxena N, Kumar S, Sharma MK, Mathur SP (2013) Corrosion inhibition of mild steel in nitric acid media by some Schiff bases derived from anisalidine. Pol J Chem Tech 15(1):61–67
3. Toliwal SD, Jadav K, Pavagadhi T (2011) Inhibition of corrosion of mild steel in 1 N HCl solutions by Schiff base derived from non-traditional oils. Indian J Chem Tech 18(4):301–308
4. Keleş H, Keleş M (2012) Electrochemical investigation of a Schiff base synthesized by cinnamaldehyde as corrosion inhibitor on mild steel in acidic medium. Res Chem Intermed. doi:10.1007/s11164-012-0955-5
5. Gopi D, Govindaraju KM, Kavitha L (2010) Investigation of triazole derived Schiff bases as corrosion inhibitors for mild steel in hydrochloric acid medium. J Appl Electrochem 40(7):1349–1356
6. Hosseini SMA, Azimi A (2008) The inhibition effect of the new Schiff base, namely 2,2′-[bis-*N*(4-choloro benzaldimin)]-1,1′-dithio against mild steel corrosion. Mater Corros 59(1):41–45
7. John S, Joseph A (2012) Electro analytical, surface morphological and theoretical studies on the corrosion inhibition behavior of different 1,2,4-triazole precursors on mild steel in 1 M hydrochloric acid. Mater Chem Phys 133:1083–1091
8. Khaled KF, Abdel Shafi NS (2013) Chemical and electrochemical investigations of L-arginine as corrosion inhibitor for steel in hydrochloric acid solutions. Int J Electrochem Sci 8:1409–1421
9. Martinez S, Štagljar I (2003) Correlation between the molecular structure and the corrosion inhibition efficiency of chestnut tannin in acidic solutions. J mol Struc-Theochem 640(1–3):167–174
10. Silva AB, Elia ED, Gomes JA (2010) Carbon steel corrosion inhibition in hydrochloric acid solution using a reduced Schiff base of ethylenediamine. Corros Sci 52(3):788–793
11. Vinod PR, Joby TK, Shaju KS, Aby P (2013) Study of synergistic effect of iodide on the corrosion antagonistic behaviour of a heterocyclic phenylhydrazone in sulphuric acid medium on carbon steel. ISRN Corrosion. doi:10.1155/2013/390823
12. Racane L, Kulenovic VT, Boykin DW, Karminski-Zamola G (2003) Synthesis of new cyano-substituted bis-benzothiazolyl arylfurans and arylthiophenes. Molecules 8(3):342–348
13. AST G-31-72 (1990) Standard recommended practice for the laboratory immersion corrosion testing of metals. ASTM, Philadelphia
14. Fouda AS, Abdallah M, Medhat M (2012) Some Schiff base compounds as inhibitors for corrosion of carbon steel in acidic media. Prot Metals Phy Chem Surf 48(4):477–486
15. Govindaraju KM, Gopi D, Kavitha L (2009) Inhibiting effects of 4-amino-antipyrine based Schiff base derivatives on the corrosion of mild steel in hydrochloric acid. J Appl Electrochem 39(12):2345–2352
16. Vinod PR, Joby TK, Shaju KS, Aby P (2014) Corrosion inhibition investigations of 3-acetylpyridine semicarbazone on carbon steel in hydrochloric acid medium. Res Chem Intermed 40(8):2689–2701

17. El Azhar M, Mernari B, Traisnel M, Bentiss F, Lagrenée M (2001) Corrosion inhibition of mild steel by the new class of inhibitors [2,5-bis(n-pyridyl)-1,3,4-thiadiazoles] in acidic media. Corros Sci 43(12):2229–2238
18. Ebenso EE (2003) Synergistic effect of halide ions on the corrosion inhibition of aluminium in H_2SO_4 using 2-acetylphenothiazine. Mater Chem Phys 79(1):58–70
19. Li X, Deng S, Fu H (2009) Synergism between red tetrazolium and uracil on the corrosion of cold rolled steel in H_2SO_4 solution. Corros Sci 51(6):1344–1355
20. Ma Cafferty M, Hackerman N (1972) Double layer capacitance of iron and corrosion inhibition with polymethylene diamines. J Electrochim Soc 119(2):146–154
21. Béchamp MA (1854) De l'action des protosels de fer sur la nitronaphtaline et la nitrobenzine. nouvelle méthode de formation des bases organiques artificielles de Zinin". Annales de chimie et de physique 42:186–196
22. Umoren SA, Eduok UM, Oguzie EE (2008) Corrosion inhibition of mild steel in 1 m H_2SO_4 by polyvinyl pyrrolidone and synergistic iodide additives. Portugaliae Electrochim Acta 26(6):533–546
23. El-Shafei AA, Moussa MNH, El-Far AA (2001) The corrosion inhibition character of thiosemicarbazide and its derivatives for C-steel in hydrochloric acid solution. Mater Chem Phys 70(2):175–180
24. Sudhish KS, Eno EE (2011) Corrosion inhibition, adsorption behavior and thermodynamic properties of streptomycin on mild steel in hydrochloric acid medium. Int J Electrochem Sci 6:3277–3291
25. Cano E, Polo JL, La Iglesia A, Bastidas JMA (2004) Study on the adsorption of benzotriazole on copper in hydrochloric acid using the inflection point of the isotherm. Adsorption 10(3):219–225
26. Bentiss F, Lebrini M, Lagrenée M (2005) Thermodynamic characterization of metal dissolution and inhibitor adsorption processes in mild steel/2,5-bis(n-thienyl)-1,3,4-thiadiazoles/hydrochloric acid system. Corros Sci 47(12):2915–2931
27. Yurt A, Balaban A, Kandemir SU, Bereket G, Erk B (2004) Investigation on some Schiff bases as HCl corrosion inhibitors for carbon steel. Mater Chem Phys 85(2–3):420–426
28. Chaitra TK, Mohana KNS, Tandon HC (2015) Thermodynamic, electrochemical and quantum chemical evaluation of some triazole Schiff bases as mild steel corrosion inhibitors in acid media. J Mol Liq 211:1026–1038
29. Popova A, Christov M (2006) Evaluation of impedance measurements on mild steel corrosion in acid media in the presence of heterocyclic compounds. Corros Sci 48(10):3208–3221
30. Satapathy AK, Gunasekaran G, Sahoo SC, Amit K, Rodrigues PV (2009) Corrosion inhibition by Justicia gendarussa plant extract in hydrochloric acid solution. Corros Sci 51(12):2848–2856
31. Ferreira ES, Giacomelli C, Giacomelli FC, Spinelli A (2004) Evaluation of the inhibitor effect of L-ascorbic acid on the corrosion of mild steel. Mater Chem Phys 83(1):129–134
32. Haugstad G (2012) Atomic force microscopy: understanding basic modes and advanced applications. Wiley, USA
33. Kumar BR, Rao TS (2012) Comparative studies of morphological and microstructural properties of electrodeposited nanocrsytalline two-phase Co–Cu thin films prepared at low and high electrolyte temperatures. Dig J Nanomater Bios 7(4):1881–1889